Diffraction and rapidity gap measurements in ATLAS

Pavel Ruzicka[1] on behalf of the ATLAS Collaboration

[1]Institute of Physics of the Academy of Sciences of the Czech Republic

DOI: `http://dx.doi.org/10.3204/DESY-PROC-2012-02/72`

Pseudorapidity gap distributions in Large Hadron Collider proton-proton collisions at $\sqrt{s} = 7$ TeV are studied using a minimum bias data sample of integrated luminosity 7.1 μb^{-1}. Cross sections are measured differentially in the size $\Delta\eta^F$ of the larger of the pseudorapidity regions extending to the limits of the ATLAS acceptance, at $\eta = \pm 4.9$, in which no final state particles are produced above a transverse momentum threshold $p_{\text{T}}^{\text{cut}}$. The measurements span the region $0 < \Delta\eta^F < 8$ for $200 < p_{\text{T}}^{\text{cut}} < 800$ MeV. The measured data, at large $\Delta\eta^F$, constrain value of pomeron intercept appropriate to triple Regge models while at small $\Delta\eta^F$, data test reliability of hadronisation models in describing rapidity and transverse momentum fluctuations in final state particle production.

1 Introduction

This report is based on the ATLAS article [1] to which a reader is referred for further information. In the Minimum Bias collisions at a center-of-mass energy of $\sqrt{s} = 7$ TeV an average distance between two neighboring charged particles with transverse momentum $p_{\text{T}} > 100$ MeV is typically around 0.15 units in pseudorapidity [2]. Larger gaps between the particles can be created due to statistical fluctuations in the hadronisation process, which are exponentially suppressed [3] as a function of gap size, or by t-channel colour singlet exchange. The colour singlet exchange can be provided by electroweak or more frequently by strongly interacting states. The later processes are termed as diffractive and their phenomenological description is inspired by Regge theory where the colour singlet object is associated with pomeron [4, 5].

The Minimum Bias processes are usually decomposed into non-diffractive contribution and three different diffractive components: Single Diffractive dissociation (SD) $pp \to pX$ producing forward gap between the intact proton and dissociated system X, Double Diffractive dissociation (DD) $pp \to XY$ where central gap is produced between the two dissociated systems X and Y and Central Diffractive contribution (CD) in which final state particles are produced in the central region with intact forward protons emerging on both sides. The kinematics of the diffractive dissociation is commonly described in terms of invariant masses M_X and M_Y of the dissociated systems X and Y respectively and squared four momentum transfer t. Alternative variables to the M_X and M_Y are

$$\xi_X = \frac{M_X^2}{s} , \qquad \xi_Y = \frac{M_Y^2}{s},$$

where s is the square of the center-of-mass energy. The size of rapidity gap is closely correlated with the variables ξ_X and ξ_Y. In case of SD, ξ_X is equal to momentum fraction loss of the

intact proton and the size $\Delta\eta$ of the rapidity gap between the final state proton and the X system satisfies

$$\Delta\eta \approx -\ln \xi_X .$$

This correlation has great importance for the measurement because it enables to constrain diffractive models by measurement of the rapidity gap spectra.

2 Reconstruction of rapidity gaps

Rapidity gaps were reconstructed using the ATLAS calorimeter system and inner detector tracker. Calorimeter has been used for its large coverage $|\eta| < 4.9$. It consists of highly segmented electromagnetic ($|\eta| < 3.2$), hadronic end-cap ($1.5 < |\eta| < 3.2$) and electromagnetic/hadronic forward ($3.1 < |\eta| < 4.9$) calorimeters all of which are liquid argon sampling calorimeters. In addition, steel/scintillator hadronic tile calorimeter covers central region ($|\eta| < 1.7$).

Energy depositions of individual particles traversing material are reconstructed in the calorimeter using clustering algorithm which combines energy deposits in individual calorimeter cells. Due to electronic noise in read-out system, cell energies exhibit random fluctuations. They are well described by Gaussian distributions parameterized by standard deviation σ_{noise} for all calorimeter subsystems with the exception of the tile calorimeter, which shows non-Gaussian tails. The default clustering algorithm [6] is seeded by cells satisfying $S = E/\sigma_{\text{noise}} > 4$, implying that on average, six noisy clusters per event are reconstructed. As the rapidity gaps can extend over many units of pseudorapidity, the gap identification relies crucially on the suppression of the noise contribution. To suppress noise to acceptable levels, the clusters are considered only if they contain at least one cell outside the tile calorimeter with $S > S_{\text{th}}(\eta)$, where $S_{\text{th}}(\eta)$ is η-dependent threshold increasing from 4.8 in the forward region to 5.8 in the central region where the cell density is high. The calorimeter information is combined with the information from the Inner Detector for $|\eta| < 2.5$.

An interval in η is deemed to contain final state particles if at least one cluster in that interval passes the noise suppression requirements and has a transverse momentum above $p_{\text{T}}^{\text{cut}}$, or if there is at least one good track in the inner detector with transverse momentum above $p_{\text{T}}^{\text{cut}}$. Detector simulation showed that the lowest accessible energy with a good acceptance is for clusters with $p_{\text{T}} > 200$ MeV.

Events with colliding protons bunch crossing are selected using the Minimum Bias Trigger Scintillator (MBTS) which consists of two discs symmetrically situated 3 m away from the interaction point and covers $2.1 < |\eta| < 3.8$. The trigger has large efficiency > 99 % for events with particle produced in the MBTS acceptance region.

The reconstructed forward gap size, $\Delta\eta^F$, is defined by the larger of the two empty pseudorapidity regions extending between the edges of the detector acceptance at $\eta = 4.9$ or $\eta = -4.9$ and the nearest track or calorimeter cluster passing the selection requirements at smaller $|\eta|$. The rapidity gap size relative to $\eta = \pm 4.9$ lies in the range $0 < \Delta\eta^F < 8$, where the upper limit on the gap size is dictated by a requirement of a high trigger efficiency $> 50\%$, which rapidly decreases once the gap extends over both positive/negative MBTS counters at the same time.

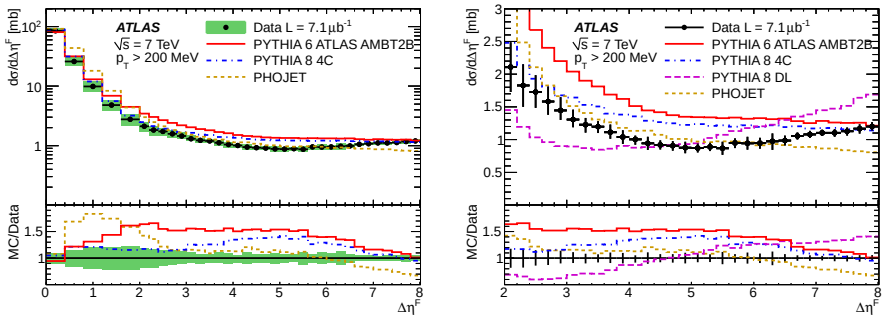

Figure 1: Inelastic cross section differential in forward gap size $\Delta\eta^F$ for particles with $p_{\mathrm{T}} >$ 200 MeV [1]. Right plot zooms into large rapidity gap region, $\Delta\eta^F > 2$.

3 Results

All the results are corrected for the detector effects to level of stable particles. Inelastic cross section differential in forward rapidity gap size, $\Delta\eta^F$, for $p_{\mathrm{T}}^{\mathrm{cut}} = 200$ MeV is shown in Fig. 1. The uncertainty of the measurement is around 8 % for large gaps, $\Delta\eta^F > 3$, and 20 % for small at $\Delta\eta^F = 1.5$. At small gaps, $\Delta\eta < 2.5$, both data and Monte Carlo (MC) models follow exponential decrease which is typical for ND events dominating this region according to all MCs. PYTHIA8 has the best agreement with the data while PHOJET overshoots the data almost by factor two due to wrong ND normalization. For large gaps, $\Delta\eta^F > 3$, a plateau in data is presented, which is attributed mainly to diffractive processes. Although the MCs reproduce the diffractive plateau, none of them describes both shape and normalization precisely over the whole range. PHOJET and PYTHIA predict that only diffractive processes contribute to cross section in the large gap region. From the right plot of the Fig. 1, which zooms into the large gaps region, it can be seen that data exhibits smaller slope than PYTHIA8 with Donnachie-Landshoff (DL) [7] but higher slope than the rest of the MCs models. The slope of the distribution for large rapidity gaps is strongly correlated with the pomeron intercept $\alpha_{I\!P}(0)$. Hence, distribution for DL model, which sets the $\alpha_{I\!P}(0) = 1.085$, grows faster for large $\Delta\eta^F$ than for the other models with $\alpha_{I\!P}(0) = 1$. This observation can be used for the determination of the pomeron intercept from data. The DL model in the PYTHIA8 has been used to fit the data in the large rapidity gaps $\Delta\eta^F > 5$. Obtained value [1]

$$\alpha_{I\!P}(0) = 1.058 \pm 0.003(\mathrm{stat.})^{+0.034}_{-0.039}(\mathrm{syst})$$

is compatible with default DL value due to large systematic uncertainty.

The distribution at small rapidity gaps is sensitive to fluctuation in hadronisation processes thus it is interesting to compare the data to other hadronisation models than Lund String model implemented in PYTHIA and PHOJET. An alternative is a cluster hadronisation model which is available in HERWIG++. The HERWIG++ Minimum Bias model tune UE7-2 is compared with data in left plot of Fig. 2. It should be emphasized that the model of minimum bias production does not contain diffraction processes and thus only exponential fall off the rapidity gap distribution is expected. Even though not containing an explicit diffractive component, HERWIG++ produces large gaps with non-exponential behavior and bump around $\Delta\eta^F = 6$. This behavior persists also when the colour reconnection (CR) model is switched-off or when

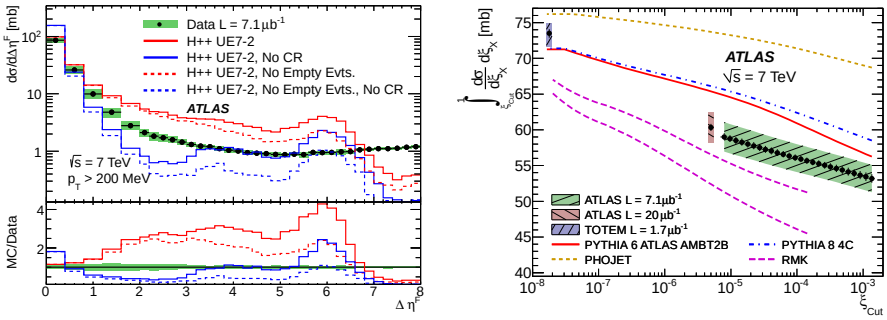

Figure 2: (Left) Inelastic differential cross section as a function of forward gap size $\Delta\eta^F$ for particles with $p_{\mathrm{T}} > 200$ MeV in HERWIG++ UE7-2 minimum bias model [1], see text for explanation. (Right) Inelastic integrated cross section as a function of minimum ξ denoted as ξ_{Cut} [1].

events with no scatterings of either the soft or semi-hard are excluded (No Empty Evts.).

The strong correlation between rapidity gaps and ξ_X makes it possible to convert the inelastic integrated cross section as a function of $\Delta\eta^F$ into an integral over the inelastic pp cross section down to some minimum value ξ_{Cut} of ξ_X i.e. perform a following transformation

$$\int_0^{\Delta\eta^F_{\mathrm{Cut}}} \frac{\mathrm{d}\sigma}{\mathrm{d}\Delta\eta^F}\mathrm{d}\Delta\eta^F \rightarrow \int_{\xi_{\mathrm{Cut}}}^{1} \frac{\mathrm{d}\sigma}{\mathrm{d}\xi_X}\,\mathrm{d}\xi_X \ .$$

This is done only by applying small correction for hadronisation effects and for including particles below $p_{\mathrm{T}} = 200$ MeV. The integrated inelastic cross section is shown as a function of ξ_{Cut} in right plot of Fig. 2. The data are compared with a previous ATLAS result [8] and with the TOTEM extraction of the full inelastic cross section [9], derived from a measurement of the elastic cross section via the optical theorem. Apart from the standard MCs models, the plot shows two versions of the KMR model [10]. PYTHIA and PHOJET fail to describe evolution of data from low to large ξ value; the fraction of low mass diffractive events is under-estimated. On the other hand, although the normalization of the KMR model is not correct, its shape exhibits better agreement with data than the rest of the models.

References

[1] ATLAS Collaboration, Eur. Phys. J., **C72** (2012) 1926.

[2] ATLAS Collaboration, New J. Phys., **13** (2011) 053033.

[3] J. Bjorken, S. Brodsky, H. J. Lu, Phys. Lett., **B286** (1992) 153.

[4] E. Feinberg, I. Pomerančuk, Suppl. Nuovo Cimento, **3** (1952) 652.

[5] G. Chew, S. Frautschi, Phys. Rev. Lett., **7** (1961) 394.

[6] W. Lampl and others, ATL-LARG-PUB-2008-002. ATL-COM-LARG-2008-003(2008).

[7] A. Donnachie, P. Landshoff, Nucl. Phys. **B244** (1984) 322.

[8] ATLAS Collaboration, Nature Comm., **2** (2011) 463.

[9] TOTEM Collaboration, EPL (Europhysics Letters), **96** (2011) 21002.

[10] M. G. Ryskin, A. D. Martin, V. A. Khoze, Eur. Phys. J., **C71** (2011) 1617.